Heat shock protein 90's mechanochemical cycle is dominated by thermal fluctuations

Christoph Ratzke, Felix Berkemeier, and Thorsten Hugel[1]

Physik-Department (E22), Institute of Medical Engineering (IMETUM), Center for NanoScience (CeNS), Center for Integrated Protein Science (CIPSM), Technische Universität München, 85748 Garching, Germany

Edited by Alan R. Fersht, Medical Research Council Laboratory of Molecular Biology, Cambridge, United Kingdom, and approved October 27, 2011 (received for review May 18, 2011)

The molecular chaperone and heat shock protein 90 (Hsp90) exists mainly as a homodimer in the cytoplasm. Each monomer has an ATPase in its N-terminal domain and undergoes large conformational changes during Hsp90's mechanochemical cycle. The three-color single-molecule assay and data analysis presented in the following allows one to observe at the same time nucleotide binding and the conformational changes in Hsp90. Surprisingly, and completely unlike the prior investigated systems, nucleotides can bind to the N-terminally open and closed state without strictly forcing the protein into a specific conformation. Both the transitions between the conformational states and the nucleotide binding/unbinding are mainly thermally driven. Furthermore, the two ATP binding sites show negative cooperativity; i.e., nucleotides do not bind independently to the two monomers. We thus reveal a picture of how nucleotide binding and conformational changes are connected in the molecular chaperone Hsp90, which has far-ranging consequences for its function and is distinct from previously investigated motor proteins.

conformational dynamics | three-color FRET | single molecule | intramolecular communication | protein structure

Molecular chaperones are proteins that assist the folding or unfolding and the assembly or disassembly of other proteins (1). A very abundant molecular chaperone in eukaryotes is the heat shock protein 90 (Hsp90) comprising around 1% of cytosolic protein (2, 3). The protein consists of two elongated monomers that have two dimerization interfaces in the N domain and in the C domain, respectively. Like motor proteins, it is an ATPase, but the mechanistic function of ATP binding and hydrolysis is still unclear. Current models assume that one ATP each binds to the N-terminal domains in the open state, followed by N-terminal closing and ATP hydrolysis in a strict succession (4)—similar to all to-date investigated motor proteins (5–9). Because of experimental limitations, it was not possible to directly observe nucleotide binding and conformational changes at the same time and thus detect the mechanochemical cycle of Hsp90. To overcome this limitation we designed a three color single-molecule Förster resonance energy transfer (smFRET) assay with alternating laser excitation (ALEX). This allows one to detect when ATP binds to which monomer and at the same time to read out the conformational state of Hsp90. Surprisingly, we find that ATP binds to the N-terminal open and close conformations, but not independently.

Therefore, our data show that the picture of a successive conformational cycle has to be replaced by stochastic transitions in-between conformations of Hsp90. Nevertheless, there is an anticorrelated communication between the N termini throughout the whole protein.

Results

ATP and ADP Bind in the N-Terminal Open and Close Conformations. We immobilize Hsp90 dimers in a microfluidic chamber of a three color FRET setup as depicted in Fig. 1*A* and described below. The N-terminal open–close dynamics is detected by FRET between Atto488 and Atto550 dyes, similar to previous experiments (10, 11). In addition, we detect ATP binding by FRET between the previous dyes and an Atto647N dye attached to the gamma phosphate group of the ATP via a hexane linker (Acceptor 2). The Atto647N-labeled nucleotide can be bound and hydrolyzed both with wild-type affinity and velocity by Hsp90 and does not bind to a secondary binding site (Figs. S1 and S2). Corrected fluorescence signals are depicted in Fig. 1 *B* and *C*, *Upper*. The partial fluorescence (PF) intensities are obtained from these traces by dividing the fluorescence intensities of acceptor 1 and 2 by the total fluorescence intensity, respectively (see *Methods*). These PFs are shown in Fig. 1 *B* and *C*, *Lower*, for acceptor 1 in black and acceptor 2 in blue. Fig. 1*B* shows a low acceptor 1 signal and sometimes a high acceptor 2 signal. Thus, this curve shows ATP binding in the N-terminally open state. Surprisingly, another type of curve also can be observed, which is shown in Fig. 1*C*; here, the acceptor 1 has high fluorescence (is closed) with occasional decrease in fluorescence coincidental with a high acceptor 2 signal. This corresponds to binding of ATP in the N-terminally closed state.

For further analysis, these PF values are plotted into two-dimensional diagrams as depicted in Fig. 1*D* (for details, see Fig. S3). For the above-described Hsp90 system, we can distinguish four areas that can be assigned to the four states depicted in Fig. 1*D*. The first area (state 1) has a high relative intensity of acceptor 1 corresponding to the N-terminally closed state without nucleotide bound. The second area (state 2) with low acceptor 1 and high acceptor 2 intensity corresponds to the N-terminally closed state with nucleotide bound and is elongated because ATP has two optional binding sites (see also Fig. 3). The third area (state 3) with low acceptor 1 and low acceptor 2 intensity represents an open state without nucleotide bound. The fourth area (state 4) finally shows also a low intensity of acceptor 1 and intermediate intensity of acceptor 2, which corresponds to an open state with nucleotide bound. This assignment of the four states was confirmed by kinetic analysis and ALEX (12, 13) as detailed below.

We probed the ATP binding at different time scales, namely 220 and 1,000 ms per data point, to overcome the limitations set by the finite lifetime of the fluorophores. At fast time scales, we mainly observe transitions between state 3 and state 4, which correspond to binding of ATP in the open state of Hsp90. In contrast, the data measured at 1,000-ms time resolution shows mainly transitions from state 1 to state 2 (namely, a surprising binding of ATP in the N-terminally closed state). Therefore, the binding and unbinding in the closed state is slower than in the open state. Transitions in-between these types of traces are rare, but occasionally take place (see Fig. S4 for an example).

The rate constants (i.e., dwell times) are then extracted by an HMM as for two color FRET (14). This algorithm searches the

Author contributions: C.R. and T.H. designed research; C.R. performed research; C.R., F.B., and T.H. analyzed data; and C.R. and T.H. wrote the paper.

The authors declare no conflict of interest.

This article is a PNAS Direct Submission.

[1]To whom correspondence should be addressed. E-mail: thorsten.hugel@ph.tum.de.

This article contains supporting information online at www.pnas.org/lookup/suppl/doi:10.1073/pnas.1107930108/-/DCSupplemental.

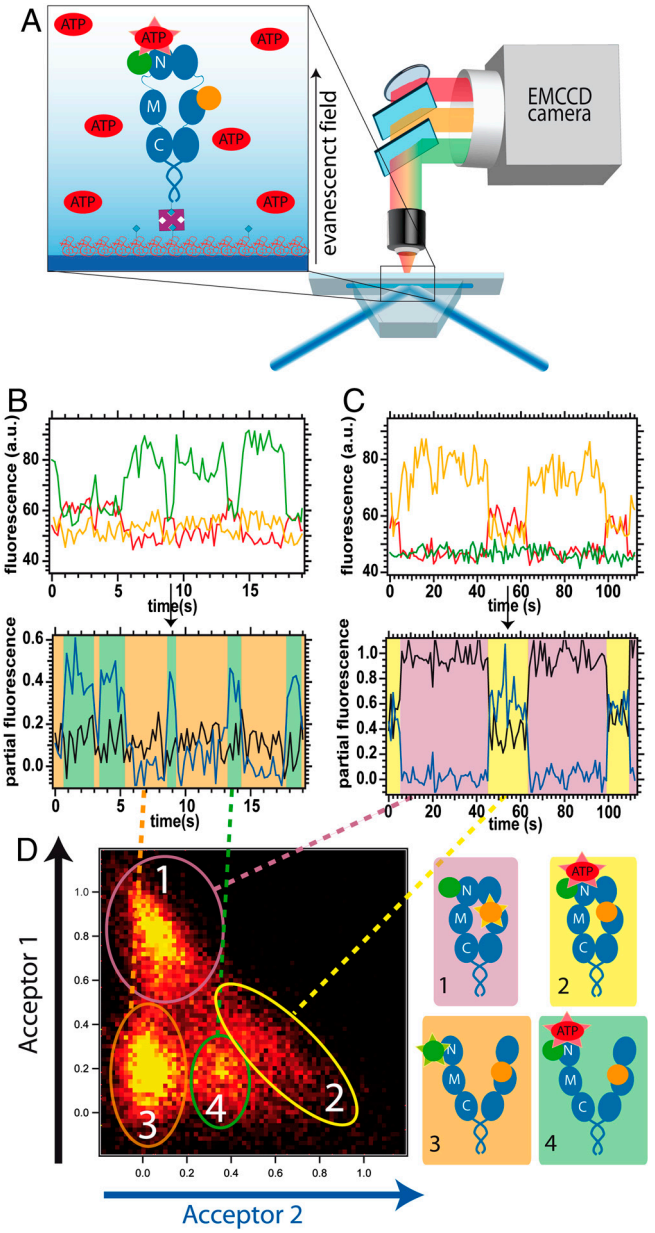

Fig. 1. Three color FRET setup and data analysis. (*A*) Hsp90 heterodimers, with the donor label (green) at position 61 of one monomer and the acceptor 1 label (orange) at position 385 of the other monomer, are fixed to the surface of a microfluidic chamber via biotin and streptavidin. ATP with the acceptor 2 label (red) at the gamma phosphate is dissolved in the buffer. The two major types of fluorescence traces are binding and unbinding in the N-terminally open (*B*) and closed (*C*) state. This leads to four states that can be separated in a two-dimensional partial intensity histogram (*D*). See main text for details.

underlying (hidden) states of a scattered signal and can easily be transferred to our multidimensional data (see *Methods* and Fig. S3). A measured example curve together with the reconstructed curve are shown in Fig. S3. The obtained dwell time distributions are plotted in cumulative histograms (10, 15), which are corrected for bias caused by the different time resolutions (see *SI Methods* for details) and superimpose very well (Fig. 2*A* for ATP and Fig. 2*B* for ADP). We find that the equilibrium dissociation constant K_d for ATP binding is little less than 1 μM for both the N-terminally open and closed states, whereas the kinetics (on- and off-rate constants) are different. After finding this unexpected ATP binding behavior, we repeated the described measurements with beta phosphate-labeled ADP. ADP binds in the open and closed states, but the binding kinetics is more than a factor of 10 faster. The fast off-rate constant for ADP points toward a short-lived ADP bound state in vivo.

ATP Binding to the Two Monomers Shows Negative Cooperativity. Hsp90 is a homodimer; therefore, in principle, two identical ATP binding sites exist. On the other hand, dimerization might induce some asymmetry in the Hsp90 dimer (16). Thus, the question arises if both binding sites can bind ATP independently or if there is some cooperativity. For the closed conformation, the answer is very clear but surprising. Binding of a second ATP would result in an increase in the high acceptor 2 signal, which was never observed (>100 traces). Thus, only one ATP binds in the closed conformation. In the open state, the situation is more difficult. If an ATP binds to the monomer that does not have the donor but the acceptor 1 dye (orange), only little energy transfer from donor to acceptor 1 to acceptor 2 (ATP, red) would take place. Such a small shift of the PF can easily be overseen, because it is close to the noise level. To overcome this limitation we used alternating excitation of the donor (green) and acceptor 1 (orange) dyes and repeated the above measurements. Now, we obtain three PF intensities simultaneously: two upon donor excitation (which are the same as in Fig. 1 above) and one additional upon acceptor 1 excitation (showing the binding of ATP to the monomer labeled with Atto550 dye). Example curves for the ATP binding in the N-terminally closed and open states are shown in Fig. 3 *C* and *D* and Fig. 3*E*, respectively. In Fig. 3*C*, both the acceptor 2 signal upon blue excitation (blue) and green excitation (red) increase because all three dyes are in close vicinity (i.e., Hsp90 is in the closed state during the ATP binding).

In the open state of Hsp90, two types of curves are obtained: one showing ATP binding to the monomer with the Atto488 dye (Fig. 3*E*) and the other one binding to the monomer labeled with Atto550 (Fig. 3*D*).

The three PF signals can be plotted in a 3D histogram. For simplification, we show the projections into 2D in various directions and separate ATP binding in the closed (Fig. 3, *Left* column) and open (Fig. 3, *Right* column) state. Fig. 3 *A* and *B* show projections onto the acceptor 1 and acceptor 2 plane. As expected, we observe the same areas, transitions, and states as in Fig. 1*D*. But now we have in addition the projection onto the ALEX (acceptor 2 upon green excitation) and acceptor 2 plane (Fig. 3*F* and Fig. 3*G*). Here, state 3 clearly separates into the two different states 3a and 3b, which could not be distinguished before without ALEX. They represent the N-terminal open state without ATP and with ATP bound to the monomer that bears the Acceptor 1 dye, respectively. On the other hand, state 4 should split into two different states (4a and 4b) if two ATPs could bind at the same time in the N-terminal open state (the center of area 4b is given by the vectorial sum of 3b and 4a, the cases where only one ATP is bound). If the two binding sites would bind ATP independently, we would observe two ATPs bound at the same time in around 6% of the time. These 6% are obtained by squaring the probability of having one ATP bound to a Hsp90 monomer (see *SI Methods* for details). This value is obtained from hidden Markov analysis. An error can therefore not directly be estimated, but 10% is definitely more than enough (in particular with the small errors of the fits in Fig. 2). The 6% would translate into more than 100(±10) data points somewhere around the center of area 4b (for the ATP concentration of 200 nM used here). From the more than 2,000 data points, only around 10 lie in the area 4b. These data points even lie at the edge of that area, which makes scattering from the other states quite likely and marks our estimate as an upper limit for the amount of double-bound ATP. We can therefore conclude that only very rarely (or even never) are two ATPs bound at the same time in the open state (<1%) and that the N-terminal nucleotide binding sites thus show negative cooperativity. In other words, they have to communicate not only

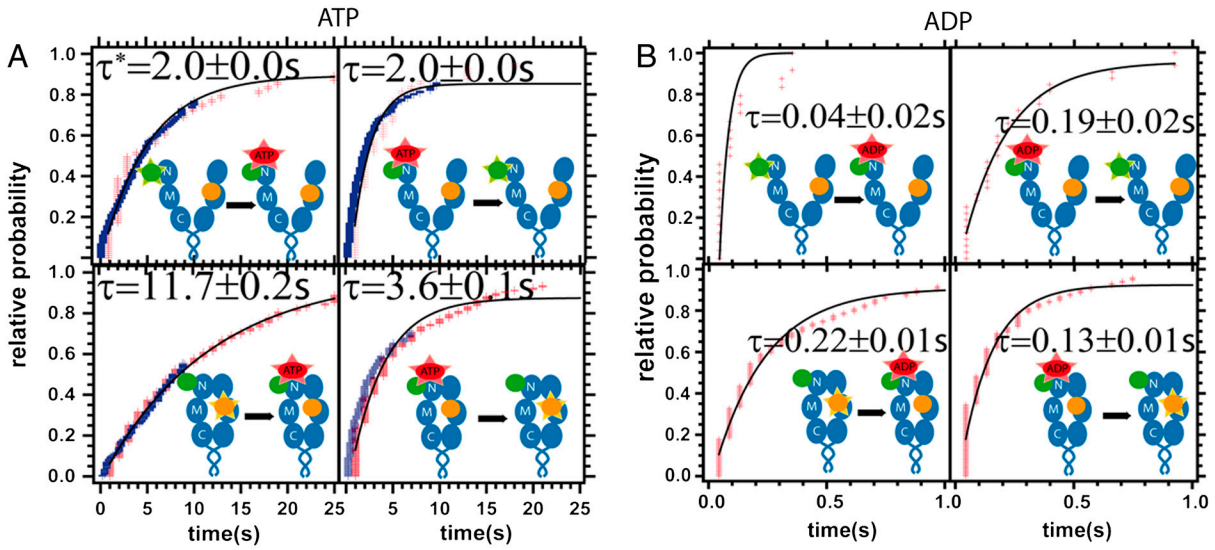

Fig. 2. Binding and release kinetics of ATP and ADP. (*A*) The binding of ATP was measured with a time resolution of 220 ms (blue) and 1,000 ms (red). The obtained dwell times were corrected for the bias caused by the different time resolutions and plotted as cumulative histograms (for details see *SI Methods*); they superimpose very well. Binding and release are faster in the open state than in the closed state. The dwell time for the ATP free state (*Upper Left*) from the graph is 6 s, which results in a corrected dwell time of 2 s taking into account the fact that binding of ATP to the monomer not bearing the Atto488 dye does not result in a measurable signal (for details see *SI Methods*). Binding and release of ADP (*B*) is more than 10 times faster than that of ATP, which resulted in a worse signal-to-noise ratio and therefore less good data (the rates are at the limit of the time resolution of our setups).

in the closed, but also in the open conformation. This in turn requires a communication through the whole protein via the C-terminal dimerization interface.

Although our measurements show strong negative cooperativity, we have to mention that at higher ATP concentrations binding of two ATPs is not unlikely. The $K_{d,1}$ for the first ATP binding in the open state is around 0.2 μM, whereas the $K_{d,2}$ for the binding of the second ATP is larger than 10 μM (the procedure is explained in *SI Methods*). This $K_{d,2}$ has to be regarded as lower limit because the amount of data points in area 4b is an upper limit, as pointed out above.

The N Terminus Is Likely More Extended than Given by the Crystal Structure. An analysis of the various fluorescence intensities allows a good estimate of the distances in-between the dyes (this nontrivial analysis is summarized in *Methods* and detailed in *SI Methods*). From the above measurements, we have two independent measurements of the distance between donor and acceptor 1 in the closed and three independent measurements in the open state. The obtained mean distances are 4.2 nm for the closed and 6.7 nm for the open state, which fit well with the estimated distances from the crystal structure of 4.2 nm for the closed and around 7.0 nm for the open state (Protein Data Bank ID codes 2CGE and 2CG9) (17) (Fig. 3*J*) and suggest an uncertainty of around 0.5 nm. Surprisingly, the four determined distances to the labeled ATP are around 6 nm (Table S1 and Fig. 3*J*), which is twice as much as expected (Fig. S5) and points toward a more extended N terminus than given by the crystal structure.

Discussion

Our three color single-molecule FRET setup has allowed observation of ATP and ADP binding and the underlying N-terminal conformational state of Hsp90 at the same time at the single-molecule level. Surprisingly, nucleotide binding does not cause an open–close transition of the Hsp90 N terminus and N-terminally open or closed states are both able to bind nucleotides, although with different kinetics. Because all the transition rates of the N-terminal movement under various nucleotide conditions and the nucleotide binding under various conformational conditions have been directly measured (Table S2), the whole mechanochemical cycle of Hsp90 can be reconstructed (Fig. 4*A*). Hsp90 in the absence of cochaperones and substrate proteins does not show a strict succession of states as previously assumed, but conformational transitions and nucleotide binding are driven by thermal fluctuations and therefore appear random.

Because of this complexity, bulk measurements could not measure and assign the various rate constants to the different conformational states. They only show a mixture of all the rate constants and can therefore not accurately describe the mechanochemical cycle. In contrast, our single-molecule results can reproduce the bulk stopped-flow measurements as shown in Fig. 4*B*, without the need of any fit parameter (see *Methods* for details).

Our data results in a K_d for ATP binding of little less than 1 μM, both for the open and the closed states. Bulk experiments have not yet been able to measure K_d for ATP binding for the full-length Hsp90, but for the isolated N-terminal domain. Interestingly, these values vary between 10 μM (18) and more than 100 μM (19) and are therefore higher than for the full-length Hsp90. This hints toward the middle and C-terminal domains being essential for correct ATP binding as already supposed by Weikl et al. (20).

Furthermore, the fact that ATP binds with around the same affinity to the N-terminally open and closed conformations and thus stabilizes both conformations in the same extent explains why no shift of the N-terminal conformational equilibrium occurs upon ATP addition as shown recently (10).

Further, we find that the two ATP binding sites show negative cooperativity. This asymmetric behavior is quite surprising, but it explains several past results. Thus, only one monomer must be able to bind ATP to reach full wild-type ATPase activity, whereas the second monomer is only necessary for cross-activation (16). Moreover, recent studies show an asymmetric binding of cochaperones (21). To facilitate this anticorrelated behavior between the two N termini, a long-term communication throughout the whole protein is necessary; such a long-range communication was already observed within a single monomer (11, 22–24) and can now be extended to the dimer. Higher ATP concentrations are currently inaccessible with this type of single-molecule experiment; therefore, we cannot exclude that two ATPs bind at the same time at physiological ATP concentration. Nevertheless, there is no reason to believe that the anticooperativity disappears at higher ATP concentrations.

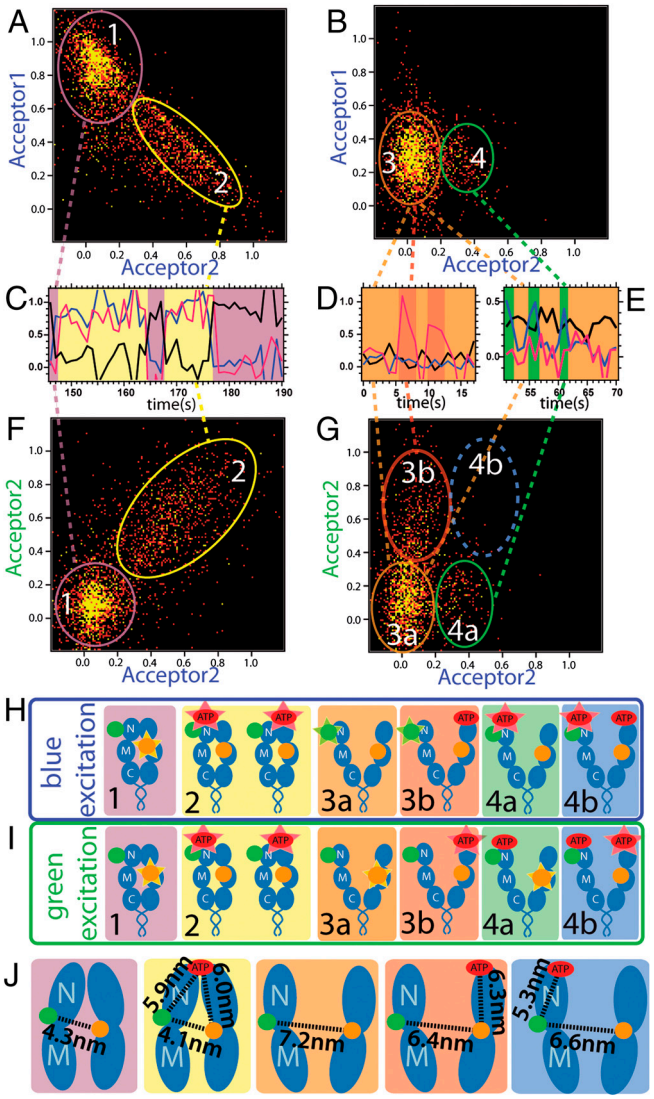

Fig. 3. Coordination of nucleotide binding and conformational changes. The donor and acceptor 1 dyes were alternating excited, which allows one to distinguish three FRET efficiencies. They can be plotted in three dimensions. We show projections onto the acceptor 1–acceptor 2 (*A* and *B*) and the ALEX (acceptor 2 upon green excitation)–acceptor 2 plane (*F* and *G*). (*C*) Example curve for ATP binding to the N-terminally closed state (red is the acceptor 2 upon green excitation). (*D* and *E*) Example curves in the open state with ATP bound at the monomer with the green (*D*) and orange (*E*) dye, respectively. Schematics of the various states that can be distinguished upon blue (*H*) and green (*I*) excitation. (*J*) Calculated distances from the fluorescence intensities between the dyes (see main text for details).

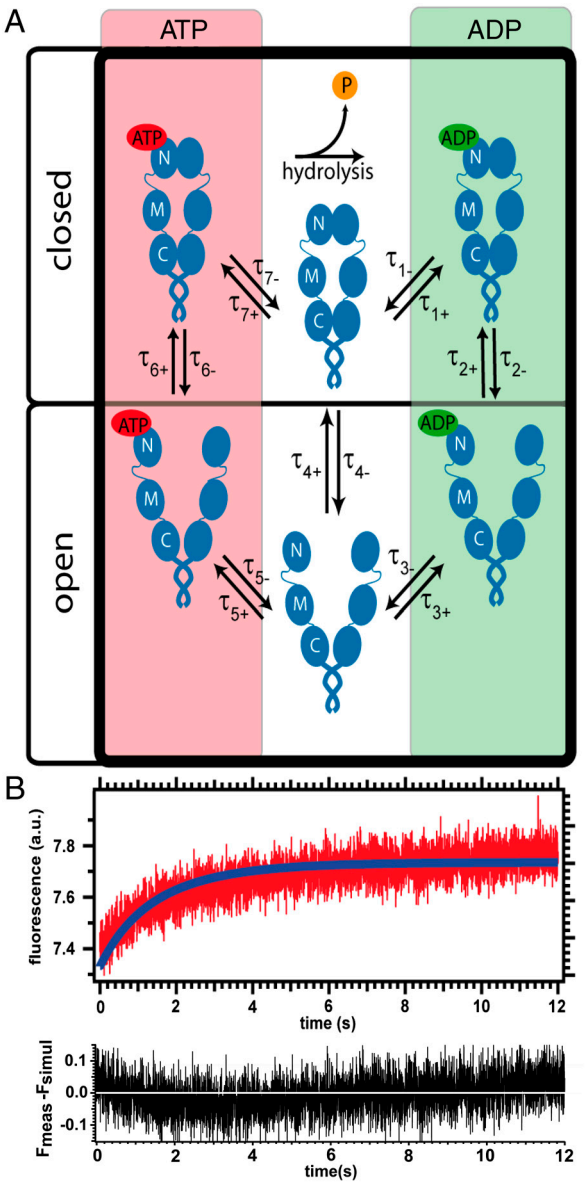

Fig. 4. Mechanochemical cycle of Hsp90. (*A*) Schematics for the mechanochemical cycle of Hsp90, where all rate constants τ_i are determined (see Table S2). Remarkably, yeast Hsp90 can transition from the N-terminal open to the closed conformation in each nucleotide state much faster than the ATP hydrolysis rate. Therefore, we have no stringent order of the different conformational and nucleotide states, but the transitions between the conformational states and nucleotide binding/unbinding are dominated by thermal fluctuations. ATP hydrolysis is the only irreversible step that slightly pushes the Hsp90 mechanochemical cycle forward, but still stays close to equilibrium. (*B*) Stopped-flow measurement of ATP binding (red curve) and simulation of the binding process using the rate constants obtained from the single-molecule measurements (blue curve). (*Lower*) The difference between the measured and the simulated curve (F_{meas} is the fluorescence of the measured, and F_{simul} is the signal of the simulated curve normalized to the measured curve). As can be seen, the single-molecule rate constants reproduce the bulk stopped-flow measurement very well considering that there is no fit parameter involved. A more detailed description of the stopped-flow measurement is given in *Methods*, and a description of the simulation is given in *SI Methods*.

Besides the kinetic information, the obtained three-color FRET data also contain structural information. The distance between the two monomers is in very good agreement with the values obtained from two-color FRET measurements (10) and the crystal structure of Hsp90 (17). Surprisingly, the distance from Hsp90 to the bound ATP is about two times as big as supposed from the crystal structure. This holds true for the N-terminally open and closed states. A little larger distance could be explained by the linker between the dye and the ATP, but even if the hexane linker between dye and ATP were completely extended, this would only account for less than 1 nm and not for the observed 3 nm. Although still unexpected, this larger extension of the N terminus of Hsp90 in solution is consistent with cryo-EM studies (25, 26).

What does our data tell us about the ATP hydrolysis? Previous studies introduced a long-lived (about 100 s) state prior to hydrolysis (also called "waiting state") to get their models consistent with the slow ATPase rate. Such a state is clearly not observed, although it would be easily detected in our single-molecule studies. We directly observe that the binding and release of ATP is much faster than the ATP hydrolysis rate; thus, ATP is bound and released several times before hydrolysis takes place. The slow ATPase rate can be explained by a high free energy barrier in-

between the ATP bound and hydrolyzed state. ATP hydrolysis itself is then an irreversible process, which is fast and specifically succeeded by ADP release (independent of the large conformational changes). This adds certain directionality to the—beside this—very stochastic Hsp90 dynamics. Because the hydrolysis rate is very slow compared to all other rates, Hsp90 in the absence of cochaperones and substrate proteins operates close to thermal equilibrium; occasional ATP hydrolysis only slightly shifts it out of equilibrium. The hydrolysis step itself happens in the closed state because N-terminal dimerization is necessary for ATP hydrolysis (19, 27).

Conclusion

Putting our results together, we have to overcome the idea of yeast Hsp90 on its own showing a strongly directed conformational cycle where one event is strictly followed by another event in a mechanochemical cycle. Instead, Hsp90 exists in a multitude of conformational states (Fig. 4*A*), which are accessible with thermal fluctuations and might be regulated by cochaperones and substrate proteins. ATP binding plays a minor role for this regulation but might be essential for the processing of substrate proteins (28).

Such a largely stochastic picture of Hsp90 has far-reaching functional consequences. The thermally driven large conformational changes allow the Hsp90 dimer to switch between different functional states without the necessity to consume energy. This enables Hsp90 to offer a variety of different substrate binding and functional states and therefore adopt efficiently to different substrate requirements. Furthermore, it can be easily externally regulated by cochaperones or posttranslational modifications, because only little external energy is needed to shift the conformational equilibrium of the protein. We speculate that the occasional energy input by ATP hydrolysis is needed for the processing or release of cochaperone or substrate proteins. In summary, we found a unique type of ATPase functionality, which offers a high conformational flexibility close to thermal equilibrium in combination with the cyclic progression of a molecular machine. This newly found mechanism is very likely relevant for many (chaperone) ATPase proteins besides Hsp90.

Methods

Single-Molecule FRET Setup All single-molecule fluorescence measurements were performed in a custom build prism-type total internal reflection fluorescence microscope similar to the one described previously (10), extended with a third excitation and detection pathway (29–31) as depicted in Fig. 1*A*. It is equipped with three lasers (473 nm Blues 50 mW Cobolt, 532 nm Compass 215 M 75 mW Coherent Inc., and 635 nm LPM635-25C 25 mW Newport) allowing for ALEX. The excitation intensity was around 3 mW for the ATP measurements and around 6 mW for the faster ADP dynamics. For the measurements with 220- and 44-ms time resolution, the sample was continuously illuminated. For the measurements with 1,000-ms time resolution, we excited the fluorophore only for 200 ms every second; therefore, the minimal time resolution of the presented measurements is 1 s, whereas the integration time for every data point is 200 ms. This delayed photo degradation of the dye and allowed observation times of several minutes. Faster underlying kinetics for the open–close movement had been excluded with measurements presented in a previous study (10).

Protein Expression and Purification. To keep the Hsp90 dimer in close proximity in the single-molecule experiments, we inserted a coiled-coil motif of the kinesin neck region of *Drosophila melanogaster* (DmKHC) to the C terminus of Hsp90 as described before (10). This construct has similar ATPase, p23 binding, and kinetics as characterized before (10). In addition, such fused Hsp90 are viable in yeast (27). Cysteine point mutations were created with the QuickChange Multi Site-Directed Mutagenesis Kit (Stratagene). We carried out protein expression and purification as described (32). We measured in the presence of 0.5 mg/mL bovine serum albumin, which slows down the N-terminal opening and closing of Hsp90 but does not affect the ATPase rate (Figs. S6 and S7). The FRET histograms of the resulting data are shown in Fig. S3, and the sum of the two histograms is depicted in Fig. 1*D*.

Stopped-Flow Measurements. The stopped-flow measurements were performed in a BioLogic SFM3 stopped-flow device at 30 °C with 2-ms time resolution. The Hsp90 61C C-terminal Zipper construct was labeled with Atto 550, and the ATP was labeled with Atto 647N at the gamma phosphate, both with a concentration of 500 nM. The excitation was at 550 nm, whereas the emission was detected from 625 to 775 nm.

Both binding partners were preincubated in the stopped-flow syringes to avoid temperature effects. Mixing of the two components led to a FRET signal and therefore an increase of the acceptor emission intensity in time. The fluorescence vs. time signal is plotted in Fig. 4.

To compare the stopped-flow data with the rates obtained from the single-molecule measurement, a computer simulation of the stopped-flow process using the rates from the single-molecule measurements were done. The concentration of free ATP is equal to the unbound Hsp90 (see above), and only one ATP binding site of Hsp90 can be occupied by ATP.

The rates of the ATP binding and unbinding of the open and closed conformations were taken from Fig. 2 and in the case of ATP binding divided by the nucleotide concentration of 200 nM because it is a second-order reaction. The rates for opening and closing with and without ATP bound are taken from ref. 10 and are around 1/5 s. For the details on the simulation, see *SI Methods*.

Three-Color FRET with ALEX Data Evaluation. For details on data evaluation, see *SI Methods*. In short, the time traces of single fluorophores were extracted from the raw data with a threshold criterion. Then, the three colors were overlaid, and the corrected PF for each color calculated as

$$\mathrm{PF}_1 = \frac{\gamma_1(I_{A1} - \beta_1 I_D)}{I_D + \gamma_1(I_{A1} - \beta_1 I_D) + \gamma_2(I_{A2} - \beta_2 I_D)}, \quad [1]$$

$$\mathrm{PF}_2 = \frac{\gamma_2(I_{A2} - \beta_2 I_D)}{I_D + \gamma_1(I_{A1} - \beta_1 I_D) + \gamma_2(I_{A2} - \beta_2 I_D)}, \quad [2]$$

$$\mathrm{PF}_\mathrm{d} = \frac{I_d}{I_D + \gamma_1(I_{A1} - \beta_1 I_D) + \gamma_2(I_{A2} - \beta_2 I_D)} = 1 - (\mathrm{PF}_1 + \mathrm{PF}_2), \quad [3]$$

and

$$E^{\mathrm{FRET}}_{\mathrm{ALEX}} = \frac{\gamma_2(I_{A2}^{532\ \mathrm{nm}} - \beta_3 I_{A1}^{532\ \mathrm{nm}})}{\gamma_1 I_{A1}^{532\ \mathrm{nm}} + \gamma_2(I_{A2}^{532\ \mathrm{nm}} - \beta_3 I_{A1}^{532\ \mathrm{nm}})}. \quad [4]$$

$\mathrm{PF}_{1/2}$ is the PF of acceptor 1 and 2, respectively. PF_d is the PF of the donor, and $E^{\mathrm{FRET}}_{\mathrm{ALEX}}$ is the PF of acceptor 2 upon direct excitation of acceptor 1. I_D and I_{A1} and I_{A2} are the donor and acceptor intensities at excitation of the donor dye, and $I_{A1}^{532\ \mathrm{nm}}$ and $I_{A2}^{532\ \mathrm{nm}}$ are the intensities of acceptor 1 and 2 upon excitation of the acceptor 1 dye, respectively. The βs are correction factors for the cross-talk in-between the channels. $\gamma_{1/2}$ are correction factors that take the different quantum efficiencies of the dyes and the different detection sensitivity of the setup for the three dyes into account.

The obtained two FRET efficiencies (every single data point) are then cumulated into a two-dimensional histogram as shown in Fig. 1*D*. To extract the dwell times HMM was used. In detail, we used the Viterbi algorithm (33) as described recently (14). As a distribution function for every state, a two-dimensional Gaussian function was used.

The rate constants for the transitions were then determined from these reconstructed FRET traces as detailed in *SI Methods*. Importantly, the obtained "effective" decay times ($1/k_{\mathrm{eff}}$) are not exactly the inverse of the rate constant k of one state to another, because the obtained effective rate constant k_{eff} is the sum of all rate constants depopulating the starting state—for four states, this can be up to three rate constants k_i (see *SI Methods* for details).

Fortunately, the binding and unbinding rates of the nucleotides are at least an order of magnitude faster than the conformational changes. Therefore, there is only one dominant pathway for the depopulation of every state, and the amplitude becomes close to one, which directly allows extracting the rate constants in our case. The kinetics can therefore be fitted with a monoexponential function.

Nucleotide binding itself is in general a second-order process, but because the nucleotide concentration is 200 nM and therefore much higher than the protein concentration (less than 1 nM), it can be regarded as constant and we have a pseudo first-order reaction to obtain the rate constants:

$$\frac{\partial N_{ab}}{\partial t} = -kN_aN_b = -k_{\mathrm{eff}}N_b. \quad [5]$$

N_a and N_b are the concentration of ATP and Hsp90, respectively. N_{ab} is the concentration of the bound complex.

Distance Information from Three-Color FRET Data. For two-dye systems, the distance between the two dyes can be estimated by (34)

$$d = R_0 \sqrt[6]{\frac{1}{\tau_D k_{\mathrm{FRET}}}}. \quad [6]$$

R_0 is the Förster distance, τ_D is the fluorescence lifetime in the absence of acceptor dye, and k_{FRET} is the rate of energy transfer between the dyes.

In the case of multicolor FRET, the single FRET efficiencies (e.g., the efficiency of the energy transfer from one dye to another dye) cannot directly be measured, because the signal results from the sum of all energy transfers (13, 35). The rate constants therefore have to be recovered as detailed in *SI Methods*. In short: If the intensities I are all corrected fluorescence intensities as in Eqs. **1–4**), the fluorescence intensity of the Donor is given by

$$I_D = Q_d N_d. \quad [7]$$

N_d is the number of absorbed photons and Q_d is the effective quantum efficiency in the presence of FRET of the donor:

$$Q_d = \frac{k_{\mathrm{rad}}}{k_{\mathrm{rad}} + k_{\mathrm{nonrad}} + \sum_i k^i_{\mathrm{FRET}}}. \quad [8]$$

k_{rad} is the radiation rate of the donor, k_{nonrad} is the nonradiative depopulation, and k^i_{FRET} is the FRET rate from the donor to the ith acceptor.

For the first acceptor, we have, accordingly,

$$I_{A1} = Q_{a1} N_{a1} = Q_{a1} \frac{k^{d\to a1}_{\mathrm{FRET}}}{\sum_j k^j_{d\to}} N_d, \quad [9]$$

where $k^{d\to a1}_{\mathrm{FRET}}$ is the FRET rate from donor to acceptor one and $\sum_j k^j_{d\to}$ are all rates that depopulate the excited state of the donor. FRET from acceptor 1 back to the donor is negligible, because of the very small overlap of the spectra.

For the second acceptor, we have, accordingly,

$$I_{A2} = Q_{a2} N_{a2} = Q_{a2} \left(\frac{k^{d\to a2}_{\mathrm{FRET}}}{\sum_j k^j_{d\to}} N_d + \frac{k^{a1\to a2}_{\mathrm{FRET}}}{\sum_k k^k_{a1\to}} N_{a1} \right). \quad [10]$$

The expression for PF (Eqs. **1–4**) can now be expressed in terms of these intensities and solved for the FRET rates, which can then be used in Eq. **6** to obtain the distances (see *SI Methods* for a complete derivation):

$$k^{d\to a1}_{\mathrm{FRET}} = -[\mathrm{PF}_1 k^d_{\mathrm{rad}} (k^{a1}_{\mathrm{rad}} \tau_d E^{\mathrm{FRET}}_{\mathrm{ALEX}} - k^{a1}_{\mathrm{rad}} \tau_d - E^{\mathrm{FRET}}_{\mathrm{ALEX}} Q^{nf}_{a1})] / [Q^{nf}_{a1} k^{a1}_{\mathrm{rad}} \tau_d \times (\mathrm{PF}_2 E^{\mathrm{FRET}}_{\mathrm{ALEX}} - \mathrm{PF}_2 + \mathrm{PF}_1 E^{\mathrm{FRET}}_{\mathrm{ALEX}} - \mathrm{PF}_1 - E^{\mathrm{FRET}}_{\mathrm{ALEX}} + 1)], \quad [11]$$

$$k^{d\to a2}_{\mathrm{FRET}} = -[(\mathrm{PF}_2 k^{a1}_{\mathrm{rad}} \tau_d E^{\mathrm{FRET}}_{\mathrm{ALEX}} - \mathrm{PF}_2 k^{a1}_{\mathrm{rad}} \tau_d + \mathrm{PF}_1 Q^{nf}_{a2} E^{\mathrm{FRET}}_{\mathrm{ALEX}}) \times k^d_{\mathrm{rad}}] / [(\mathrm{PF}_2 E^{\mathrm{FRET}}_{\mathrm{ALEX}} - \mathrm{PF}_2 + \mathrm{PF}_1 E^{\mathrm{FRET}}_{\mathrm{ALEX}} - \mathrm{PF}_1 - E^{\mathrm{FRET}}_{\mathrm{ALEX}} + 1) \tau_d k^{a1}_{\mathrm{rad}} Q^{nf}_{a2}], \quad [12]$$

and

$$k^{a1\to a2}_{\mathrm{FRET}} = \frac{E^{\mathrm{FRET}}_{\mathrm{ALEX}}}{(E^{\mathrm{FRET}}_{\mathrm{ALEX}} - 1)\tau_d}. \quad [13]$$

Eqs. **11–13** depend only on PF_1, PF_2, and $E^{\mathrm{FRET}}_{\mathrm{ALEX}}$ (which can be directly read from the maxima in the three-dimensional histogram—or from its projections depicted in Fig. 3) and on parameters given by the provider of the dye. Q^{nf} are the quantum efficiencies in the absence of FRET (which are usually given by the provider). This general treatment is not limited to a three-color case but can be extended to any number of dyes. Our approach is complementary to the one developed by Lee et al. (13), which is based upon intensity ratios instead of rates. Both approaches finally lead to correct distance information.

Because there is some uncertainty in the used values for the quantum efficiency, radiative lifetime, and the kappa factor (10), the values of the distances should be only taken as estimates. Because every distance in our system has been measured independently at least two times, we can estimate an uncertainty between 0.5 and 1 nm.

ACKNOWLEDGMENTS. Helpful discussions with Johannes Buchner, William Eaton, Roland Netz, Matthias Rief, Erich Sackmann, Attila Szabo, and Klaus Schulten are gratefully acknowledged. This work was supported by the German Science Foundation (Hu997/9-1, SFB 863) and the Nanosystems Initiative Munich. C.R. is supported by the International Doctorate Program NanoBioTechnology of the Elitenetzwerk Bayern.

1. Hartl FU, Hayer-Hartl M (2002) Molecular chaperones in the cytosol: From nascent chain to folded protein. *Science* 295:1852–1858.
2. Csermely P, Schnaider T, Soti C, Prohaszka Z, Nardai G (1998) The 90-kDa molecular chaperone family: Structure, function, and clinical applications. A comprehensive review. *Pharmacol Ther* 79:129–168.
3. Welch WJ, Feramisco JR (1982) Purification of the major mammalian heat shock proteins. *J Biol Chem* 257:14949–14959.
4. Mayer MP, Prodromou C, Frydman J (2009) The Hsp90 mosaic: A picture emerges. *Nat Struct Mol Biol* 16:2–6.
5. Schliwa M, Woehlke G (2003) Molecular motors. *Nature* 422:759–765.
6. Bustamante C, Chemla YR, Forde NR, Izhaky D (2004) Mechanical processes in biochemistry. *Annu Rev Biochem* 73:705–748.
7. Adachi K, et al. (2007) Coupling of rotation and catalysis in F(1)-ATPase revealed by single-molecule imaging and manipulation. *Cell* 130:309–321.
8. Asbury CL, Fehr AN, Block SM (2003) Kinesin moves by an asymmetric hand-over-hand mechanism. *Science* 302:2130–2134.
9. Michaelis J, Muschielok A, Andrecka J, Kugel W, Moffitt JR (2009) DNA based molecular motors. *Phys Life Rev.*
10. Mickler M, Hessling M, Ratzke C, Buchner J, Hugel T (2009) The large conformational changes of Hsp90 are only weakly coupled to ATP hydrolysis. *Nat Struct Mol Biol* 16:281–286.
11. Ratzke C, Mickler M, Hellenkamp B, Buchner J, Hugel T (2010) The dynamics of hsp90 C-terminal dimerization is an important part of its conformational cycle. *Proc Natl Acad Sci USA* 107:16101–16106.
12. Kapanidis AN, et al. (2004) Fluorescence-aided molecule sorting: Analysis of structure and interactions by alternating-laser excitation of single molecules. *Proc Natl Acad Sci USA* 101:8936–8941.
13. Lee NK, et al. (2007) Three-color alternating-laser excitation of single molecules: Monitoring multiple interactions and distances. *Biophys J* 92:303–312.
14. McKinney SA, Joo C, Ha T (2006) Analysis of single-molecule FRET trajectories using hidden Markov modeling. *Biophys J* 91:1941–1951.
15. Gebhardt JC, Clemen AE, Jaud J, Rief M (2006) Myosin-V is a mechanical ratchet. *Proc Natl Acad Sci USA* 103:8680–8685.
16. Richter K, Muschler P, Hainzl O, Buchner J (2001) Coordinated ATP hydrolysis by the Hsp90 dimer. *J Biol Chem* 276:33689–33696.
17. Ali MM, et al. (2006) Crystal structure of an Hsp90-nucleotide-p23/Sba1 closed chaperone complex. *Nature* 440:1013–1017.
18. Richter K, Reinstein J, Buchner J (2002) N-terminal residues regulate the catalytic efficiency of the Hsp90 ATPase cycle. *J Biol Chem* 277:44905–44910.
19. Prodromou C, et al. (2000) The ATPase cycle of Hsp90 drives a molecular 'clamp' via transient dimerization of the N-terminal domains. *EMBO J* 19:4383–4392.
20. Weikl T, et al. (2000) C-terminal regions of Hsp90 are important for trapping the nucleotide during the ATPase cycle. *J Mol Biol* 303:583–592.
21. Li J, Richter K, Buchner J Mixed Hsp90-cochaperone complexes are important for the progression of the reaction cycle. *Nat Struct Mol Biol* 18:61–66.
22. Retzlaff M, et al. (2009) Hsp90 is regulated by a switch point in the C-terminal domain. *EMBO Rep.*
23. Phillips JJ, et al. (2007) Conformational dynamics of the molecular chaperone Hsp90 in complexes with a co-chaperone and anticancer drugs. *J Mol Biol* 372:1189–1203.
24. Graf C, Stankiewicz M, Kramer G, Mayer MP (2009) Spatially and kinetically resolved changes in the conformational dynamics of the Hsp90 chaperone machine. *EMBO J* 28:602–613.
25. Bron P, et al. (2008) Apo-Hsp90 coexists in two open conformational states in solution. *Biol Cell* 100:413–425.
26. Southworth DR, Agard DA (2011) Client-loading conformation of the Hsp90 molecular chaperone revealed in the cryo-EM structure of the human Hsp90:Hop complex. *Mol Cell* 42:771–781.
27. Pullen L, Bolon DN (2011) Enforced N-domain proximity stimulates HSP90 ATPase activity and is compatible with function in vivo. *J Biol Chem* 286:11091–11098.
28. Walerych D, et al. (2010) ATP binding to Hsp90 is sufficient for effective chaperoning of p53 protein. *J Biol Chem* 285:32020–32028.
29. Clamme JP, Deniz AA (2005) Three-color single-molecule fluorescence resonance energy transfer. *Chemphyschem* 6:74–77.
30. Ross J, et al. (2007) Multicolor single-molecule spectroscopy with alternating laser excitation for the investigation of interactions and dynamics. *J Phys Chem B* 111:321–326.
31. Roy R, Kozlov AG, Lohman TM, Ha T (2009) SSB protein diffusion on single-stranded DNA stimulates RecA filament formation. *Nature* 461:1092–1097.
32. Richter K, Buchner J (2001) Hsp90: Chaperoning signal transduction. *J Cell Physiol* 188:281–290.
33. Viterbi AJ (1967) Error bounds for convolution codes and an asymptotically optimum decoding algorithm. *IEEE Trans Inf Theory* 13:260–269.
34. Förster T (1948) Zwischenmolekulare Energiewanderung und Fluoreszenz. *Ann Phys* 437:55–75.
35. Lee J, et al. (2010) Single-molecule four-color FRET. *Angew Chem Int Ed Engl* 49:9922–9925.